RESEARCH ARTICLE

Key Points:
- Antarctic calving-size distribution affects iceberg trajectories and melt patterns.
- Increasing iceberg size leads to an increase in the westward iceberg freshwater transport in the Antarctic Counter Current
- Iceberg freshwater transport influences regional hydrography and sea-ice formation around Antarctica

The effects of Antarctic iceberg calving-size distribution in a global climate model

A. A. Stern[1], A. Adcroft[1], and O. Sergienko[1]

[1]Geophysical Fluid Dynamics Laboratory, Princeton University, Princeton, New Jersey, USA

Abstract Icebergs calved from the Antarctic continent act as moving sources of freshwater while drifting in the Southern Ocean. The lifespan of these icebergs strongly depends on their original size during calving. In order to investigate the effects (if any) of the calving size of icebergs on the Southern Ocean, we use a coupled general circulation model with an iceberg component. Iceberg calving length is varied from 62 m up to 2.3 km, which is the typical range used in climate models. Results show that increasing the size of calving icebergs leads to an increase in the westward iceberg freshwater transport around Antarctica. In simulations using larger icebergs, the reduced availability of meltwater in the Amundsen and Bellingshausen Seas suppresses the sea-ice growth in the region. In contrast, the increased iceberg freshwater transport leads to increased sea-ice growth around much of the East Antarctic coastline. These results suggest that the absence of large tabular icebergs with horizontal extent of tens of kilometers in climate models may introduces systematic biases in sea-ice formation, ocean temperatures, and salinities around Antarctica.

1. Introduction

Freshwater discharge from the Antarctic Ice Sheet into the Southern Ocean takes the form of both sub-ice-shelf melting and iceberg calving. Basal melting of ice shelves results in meltwater being injected at the depth of the ice-shelf bases and rising because of its positive buoyancy [*MacAyeal*, 1984; *Jenkins*, 1991]. This upwelling of meltwater plays a role in driving the circulation in the sub-ice-shelf cavities. Once the meltwater exits the ice-shelf cavity, it can affect local sea-ice formation, production of dense water, and ocean biological activity [e.g., *Dieckmann et al.*, 1986; *Nicholls et al.*, 2009].

Similarly, icebergs play an important role in influencing the ocean around them. Subsurface iceberg melting can drive upward-moving buoyant plumes around the iceberg perimeter, which entrain water as they rise [e.g., *Neshyba*, 1977; *Stephenson et al.*, 2011]. The bottom layers of icebergs are rich in iron and other nutrients from being in contact with Antarctic bedrock. Melting icebergs can increase ocean iron concentrations, stimulating biological activity, and leading to local enhancements in the rates of carbon sequestration [*Smith et al.*, 2007; *Vernet et al.*, 2012; *Biddle et al.*, 2015]. Large tabular icebergs can disrupt flow patterns and alter ocean temperatures and salinities [*Grosfeld et al.*, 2001; *Robinson et al.*, 2012; *Stern et al.*, 2015]. As with sub-ice-shelf melting, the presence of icebergs can also influence the sea-ice and deep water formation [*Nøst and Østerhus*, 1998; *Dinniman et al.*, 2007; *Kusahara et al.*, 2011].

Recent studies by *Rignot et al.* [2013] and *Depoorter et al.* [2013] estimate an Antarctic calving flux of 1265 ± 141 Gt/yr, and 1321 ± 44 Gt/yr, respectively. These calving fluxes are modestly smaller than the estimates of sub-ice-shelf melting (1500 ± 237 Gt/yr and 1454 ± 174 Gt/yr, respectively) from the same studies. The division of freshwater flux into melting and calving could have implications for the global climate system, since while basal melting of ice shelves drives changes in the local hydrography, the long distances traveled by icebergs mean that icebergs can affect the ocean far from their calving origins.

Global ocean models with iceberg components [*Bigg et al.*, 1997; *Gladstone et al.*, 2001] show very different effects between sub-ice-shelf melting and iceberg melting. Numerical experiments run with and without icebergs show that introducing icebergs into a fully coupled general circulation model (GCM) results in significant changes in the modeled ocean and sea-ice conditions around Antarctica [*Jongma et al.*, 2009; *Martin and Adcroft*, 2010; *Marsh et al.*, 2015]. These changes are driven by both the cooling and freshening effects of icebergs [*Jongma et al.*, 2009]. In simulations with icebergs, the icebergs carry freshwater away from the coast in frozen form, causing warm salty anomalies at the coastline relative to simulations where the same

quantity of meltwater is injected directly at the coast [*Martin and Adcroft*, 2010; *Marsh et al.*, 2015]. These anomalies cause reduced sea-ice concentration and thickness, and can also lead to increased deep water formation. These modeling studies highlight the important role that icebergs play in the climate system, and they also show that models that do not include an iceberg component are effectively introducing systematic biases [*Martin and Adcroft*, 2010].

Despite these modeling efforts, the current generation of iceberg models are not yet able to represent the full range of iceberg sizes observed in nature. Iceberg sizes in the real-world ocean vary over a wide range of scales from growlers ($L_0 \leq 10$ m) to "giant" tabular icebergs ($L_0 \geq 10$ km). Giant icebergs form by calving off floating ice shelves in large and infrequent calving events [*Fricker et al.*, 2002], while smaller icebergs form by more frequent smaller calving events, breaking fragments off the sides of larger icebergs [*Wagner et al.*, 2014], or in rare events, as a result of ice-shelf disintegration [*Scambos et al.*, 2004].

The calving-size distributions used in the current generation of iceberg models are based on iceberg-size distributions calculated from ship-based measurements [*Gladstone et al.*, 2001; *Budd et al.*, 1980; *Orheim*, 1980; *Wadhams*, 1988]. More recently, satellite observations have been used to measure iceberg-size distributions [*Tournadre et al.*, 2008; *Stuart and Long*, 2011; *Tournadre et al.*, 2015], and recent results suggest that the Southern Hemisphere iceberg area distribution follows a $-3/2$ power law (i.e., the probability $p(A)$ of a randomly selected iceberg having an area A scales like $p(A) \sim A^{-\frac{3}{2}}$) [*Tournadre et al.*, 2016]. This power law structure of iceberg-size distribution is possibly a result of the scale invariance of brittle fragmentation processes [*Astrom et al.*, 2006; *Spahn et al.*, 2014]. According to this power law distribution, icebergs larger than 100 km^2 account for more that 89% of the total iceberg volume [*Tournadre et al.*, 2016]. In contrast, the icebergs currently represented in GCM's (in this study and previous modeling studies) only represent icebergs with an area ≤ 3.5 km^2, for reasons discussed in section 4. While it is known that the calving size of an iceberg strongly affects its trajectory and hence, its melting pattern [*Silva et al.*, 2006], it is not yet fully understood how Antarctic and Greenlandic calving-size distributions impact the climate system (or the behavior of climate models), and it is still unclear what biases are being introduced into GCMs by omitting giant icebergs.

In this paper, we study how the calving size of icebergs affects their trajectories and melt patterns, and how this impacts the sea-ice formation and ocean temperatures around Antarctica. This question is investigated by performing numerical experiments representing icebergs calved at different sizes, and comparing the results to simulations where the equivalent freshwater flux is discharged into the ocean in liquid form directly at the Antarctic coastline. These experiments illuminate several aspects: first, they give insights into how iceberg size influences ocean and sea-ice conditions around Antarctica, and how the freshwater transported in larger icebergs affects regional sea-ice production around Antarctica. Second, analysis of simulations with increasing iceberg calving size provides the sign and structure of biases that may be introduced by current climate models that omit giant icebergs, which account for the vast majority of real-world iceberg mass.

The manuscript is organized as follows: section 2 describes the model and the numerical experiments used in this study. Section 3 presents model results, and discusses how iceberg calving size impacts iceberg trajectories and melt patterns, and sea-ice and ocean conditions around Antarctica. In section 4, we consider how the open-ocean iceberg-size distribution in the model compares to real-world observations, and in light of this, we discuss what calving-size distribution should be used in climate models. Section 5 contains concluding remarks.

2. Model Setup

2.1. GFDL CM2G Coupled Climate Model With an Iceberg Component
All numerical experiments in this study are performed with the Geophysical Fluid Dynamics Laboratory (GFDL) coupled general circulation model CM2G [*Dunne et al.*, 2012]. The coupled model components include the AM2 atmosphere model, MOM6 ocean model, SIS2 sea-ice model, and LM3 land model. The atmospheric model is run on a $2° \times 2°$ global grid. The ocean model uses a $1° \times 1°$ grid, and 63 isopycnal layers in the vertical. More details about the model can be found in *Delworth et al.* [2006] and *Dunne et al.* [2012].

In addition to the ocean, atmosphere, land, and sea-ice model components, the model includes an iceberg component [*Martin and Adcroft*, 2010], based on the equations outlined in *Bigg et al.* [1997] and *Gladstone et al.* [2001]. The iceberg model stores frozen water in the form of Lagrangian point particles which melt according to parameterizations for iceberg decay. The icebergs are advected by the flow, driven by atmosphere, ocean, and sea-ice drag forces, as well as the Coriolis force and a force due to the sea surface slope. The iceberg momentum equation is given by

$$M\frac{d\vec{v}_i}{dt} = -M\vec{f}\times\vec{v}_i + \vec{\tau}_o + \vec{\tau}_a + \vec{\tau}_i + \vec{F}_r - Mg\vec{\nabla}\eta.$$ (1)

Here M is the iceberg mass, f is the Coriolis parameter, g is the gravitational acceleration, η is the sea surface height, $\vec{v}_i$ is the iceberg velocity, $\vec{\tau}_o$, $\vec{\tau}_a$, $\vec{\tau}_i$ are the forces due to oceanic, atmospheric and sea-ice drag respectively, and $\vec{F}_r$ is the force on the iceberg due to wave radiation. Using geostrophic balance the momentum equation can be rewritten as

$$M\frac{d\vec{v}_i}{dt} = -M\vec{f}\times(\vec{v}_i - \vec{v}_g) + \vec{\tau}_o + \vec{\tau}_a + \vec{\tau}_i + \vec{F}_r$$ (2)

where $\vec{v}_g$ is the geostrophic velocity of the ocean. The first term on the right-hand side of the above equation gives the effect the Coriolis force on the iceberg after the geostrophically balance part has been subtracted, and is referred to as the "Coriolis-related force" [*Gladstone et al.*, 2001].

While the iceberg location only occupies a point in space, the thermodynamics parameterizations and drag force calculations assume that the icebergs are cuboid in shape. As the icebergs drift, they "melt" according to parameterizations for iceberg decay, and their lengths, widths, and depths evolve with time. Melt occurs at the base of the iceberg due to turbulent heat flux from the ocean, and at the sides of the iceberg due to both wave erosion and buoyant convection. All melt rates are proportional to the differences between sea surface temperature and the surface freezing point, and are much reduced when the iceberg is surrounded by sea ice. Sea-ice cover also directly damps the melt due to wave erosion, which is the largest of the three decay mechanisms. Full details of the iceberg model are found in Appendix A in *Martin and Adcroft* [2010].

The full model setup used in this study is identical to the one used in *Martin and Adcroft* [2010], except for the use of a C-grid instead of B-grid discretization in the sea-ice component.

2.2. Prescribed Calving Flux and Calving-Size Distributions

We define the Antarctic frozen runoff flux, F_{FR}, as the flux of frozen freshwater from the Antarctic continent into the ocean. In this coupled model, F_{FR}, is set to be equal to the frozen precipitation over the Antarctic continent, so that the amount of freshwater in the coupled system is conserved. The frozen precipitation is instantaneously routed to the coast via hydraulic potential pathways in the land model, which determine the locations at which this frozen runoff is discharged into the ocean. Liquid runoff is also present and is handled separately.

In simulations without the iceberg module, the Antarctic frozen runoff flux is discharged into the ocean at the coastline as a liquid freshwater flux (with the corresponding latent heat flux added to the heat budget). This is done in our control simulation (referred to as CONTROL). This coastal freshwater flux is referred to as $F_{control}$. In simulations with the iceberg module, the evolution of F_{FR} is computed by the iceberg module. The flux of frozen freshwater into the iceberg module is referred to as the calving flux, F_C. Figures 1a and 1b illustrates evolution of the Antarctic frozen runoff flux in the CONTROL and ICEBERG experiments. The fluxes shown in Figure 1b are:

1. F_{FR}: flux of frozen freshwater from the Antarctic continent into the ocean.
2. $F_{control}$: flux of instantaneously melted coastal meltwater (CONTROL simulations).
3. F_C: calving flux of frozen freshwater into the iceberg module (ICEBERG simulations)
4. F_{IM}: flux of iceberg meltwater into the ocean.

In the iceberg module, the total calving flux at each location around the coast is partitioned into fluxes of icebergs in a fixed number of different size classes. "Calving size classes" refers to icebergs calving with a prescribed length, width, thickness, and mass. A maximum of 10 iceberg classes are used in this study, due to computational limitations, consistent with previous studies (Table 1). The fraction of the total calving flux which enters each iceberg class is given by a prescribed calving-size distribution. Once accumulated ice
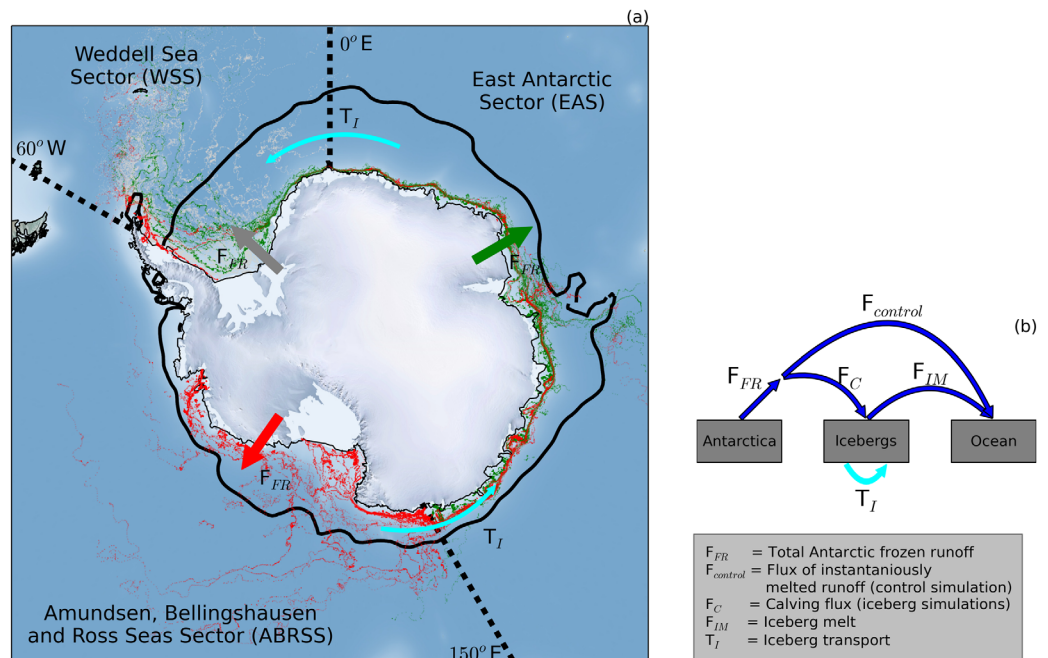
Figure 1. (a) Freshwater fluxes from Antarctica into the global ocean, and the movement of icebergs in the Antarctic Counter Current (ACoC). The black line shows the position of the northern edge of the ACoC, and the light blue arrows indicate iceberg transport between sectors (the iceberg transport through the Drake Passage is small, and is therefore not indicated). The colored dots show the positions of icebergs from the NIC large iceberg database, which calved in the ABRSS (red), EAS (green), and WWS (gray). Dashed lines separate the ABRSS, EAS, WSS sectors. (b) Redistribution of the freshwater fluxes from Antarctica into the ocean and iceberg modules. The Antarctic frozen runoff flux, F_{FR}, is instantaneously melted at the coast in the CONTROL simulation, causing a melt flux into the ocean ($F_{control}$). In the ICEBERG simulations, F_{FR} becomes a calving flux, F_C, which is diverted to the iceberg module. The calving flux enters the ocean in the form of icebergs. These icebergs move with the ocean currents that cause an iceberg freshwater transport (TI) around the Antarctic coastline, and eventually melt, causing an iceberg meltwater flux, F_{IM}, into the ocean.

mass exceeds the iceberg mass of a given class, an iceberg is created. The starting masses and thicknesses of each of the iceberg classes, as well as the calving-size distribution, are not computed in the model, they are prescribed a priori and are input parameters. The calving-size distribution is the main input parameter varied in this study, and is discussed below.

The calving length in each iceberg class, L_0, is assumed to be 1.5 times the calving width. Throughout the paper, the term "iceberg area" refers to the area of the upper surface of the iceberg. Since the modeled iceberg calving area is completely determined by the calving length, the term "calving size" is used to describe both the calving length and the calving area, while "calving-size distributions" and "iceberg-size distributions" refer to iceberg distributions by area.

Table 1. Description of the Iceberg Calving Classes Used in the Model[a]

Class	Mass (kg)	Length (m)	Area (km²)	Th (m)	Scaling
Class 1	8.8×10^7	62	0.0026	40	2000
Class 2	4.1×10^8	104	0.0072	67	200
Class 3	3.3×10^9	209	0.029	133	50
Class 4	1.8×10^{10}	426	0.12	175	20
Class 5	3.8×10^{10}	518	0.18	250	10
Class 6	7.5×10^{10}	728	0.35	250	5
Class 7	1.2×10^{11}	920	0.56	250	2
Class 8	2.2×10^{11}	1246	1.0	250	1
Class 9	3.9×10^{11}	1659	1.8	250	1
Class 10	7.4×10^{11}	2285	3.5	250	1

[a]Mass, Length, Area, and Th refer to the iceberg mass, length, area, and thickness at the time of calving. Scaling is the number of icebergs represented by one Lagrangian point particle. The iceberg mass and thickness for each class are the same as those reported in *Gladstone et al.* [2001]. The iceberg area and length for each class is calculated from the iceberg mass and thickness by assuming that the icebergs are cuboids with a length to width ratio of 1.5, using an iceberg density $\rho_i = 850$ kg/m³.

Table 2. Calving-Size Distributions[a]

Class	T_n (%)	T_{mass} (%)	G_n (%)	M_n (%)
Class 1	34.1	0.03	24	80
Class 2	27.0	1.8	12	17
Class 3	20.5	4.7	15	2.1
Class 4	10.3	9.7	18	0.4
Class 5	1.8	4.1	12	0.2
Class 6	2.4	9.3	7	0.1
Class 7	1.2	8.5	3	0.06
Class 8	1.2	14.5	3	0.03
Class 9	0.9	18.5	3	0.02
Class 10	0.1	27.6	2	0.01

[a]Class refers to the iceberg calving classes described in Table 1. T_n is the calving-size distribution used in the COMPOSITE simulation in this study. T_{mass} is the corresponding mass-weighted distribution for the COMPOSITE simulation. G_n is the calving-size distribution from *Gladstone et al.* [2001]. M_n is the calving-size distribution used in *Martin and Adcroft* [2010].

2.3. Numerical Experiments

We conduct a series of numerical experiments to examine the effect of iceberg calving size on ocean temperatures, salinities, and sea-ice conditions around Antarctica. All simulations are run for 120 years, and analysis is done using the final 60 years of the simulations, after the sea-ice and iceberg components have spun up. The results presented below are not sensitive to the number of years used for the analysis.

In the first experiment, a set of simulations is performed using icebergs in a single size class only, which we refer to as DELTA experiments. For example, the simulation named DELTA1 uses only icebergs in the smallest iceberg class with calving length $L_0 = 62$ m, while DELTA9 uses only icebergs in the iceberg class with initial length $L_0 = 1659$ m. In order to connect this experiment with past iceberg studies, we use the iceberg classes given in *Gladstone et al.* [2001]. The masses, lengths, thicknesses, and areas of the icebergs in each iceberg class are given in Table 1. Note that the maximum calving length used in this study is $L_0 = 2285$ m, which is small compared to the giant tabular icebergs ($L_0 \geq 10$ km) that are observed in the Southern Ocean.

In a second iceberg experiment, a new calving-size distribution is constructed based on $-3/2$ power law iceberg-size distribution observed by *Tournadre et al.* [2016]. This simulation is referred to as COMPOSITE (since it contains icebergs in more than one iceberg class). The calving-size distribution (T_n) and the corresponding mass-weighted distribution (T_{mass}) for the COMPOSITE simulation are shown in Table 2. The calving-size distribution gives the percent of the number of calving icebergs in each calving class, while the mass-weighted distribution gives the percent of the calving iceberg mass in each calving class. Notice that while the smallest iceberg class has 34% of icebergs by frequency, it accounts for only 0.03% of the iceberg mass. In contrast, the largest iceberg class has only 0.1% of icebergs by frequency but accounts for 27.6% of the iceberg mass.

Results from all the iceberg simulations are compared to the CONTROL simulation performed without icebergs. The time-averaged fields for CONTROL experiment are provided in the supplementary material. In the CONTROL experiment, $F_{FR} \approx 2550$ Gt/year, which agrees well with observed estimates of Antarctic freshwater flux [*Rignot et al.*, 2013; *Depoorter et al.*, 2013]. We note that although the Antarctic frozen runoff, F_{FR}, is set dynamically by the coupled model (since it is equal to the frozen precipitation over the Antarctic continent), the annual average value of F_{FR} found in all the ICEBERG simulations is within 3% of the CONTROL experiment. The primary role of icebergs is to change the spatial location of where this freshwater enters the ocean. Changes to the sea-ice and ocean properties in the various simulation are a result of this redistribution of freshwater forcing (rather than changing the total volume of freshwater).

In addition to the simulations described above, a number of simulations were run using a coupled ocean/sea-ice/iceberg model, with prescribed atmospheric forcing and a fixed (constant) calving flux. The results from these fixed calving flux simulations (not shown), are qualitatively similar to corresponding fields using the fully coupled model. This suggests that both the small differences in F_{FR} between model runs, and the seasonality in F_{FR} in the fully coupled model, do not strongly affect the results presented below.

3. Model Results

In the description of the model results below, we divide the Antarctic coastline into three sectors: Amundsen, Bellingshausen, and Ross Sea Sector (ABRSS); East Antarctic Sector (EAS); and the Weddell Sea Sector (WSS). These three sectors are shown in Figure 1a.
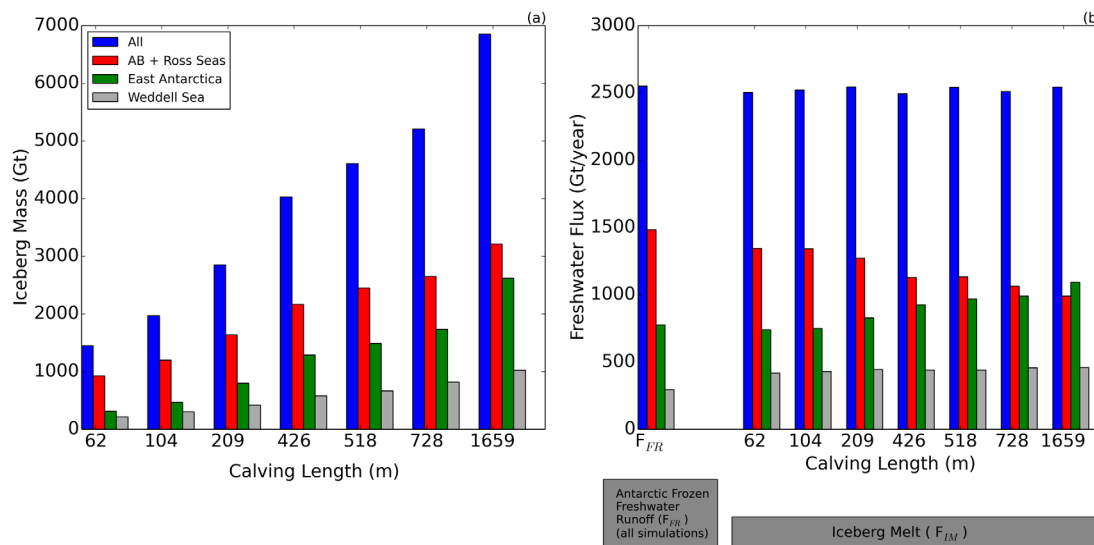
Figure 2. Equilibrated iceberg (a) mass and (b) meltwater flux (F_{IM}) for different DELTA experiments for Southern Hemisphere (blue), Weddell Sea Sector (black), Amundsen, Bellinghaus, and Ross Sea Sector (red), and East Antarctic Sector (green). The definitions of the three Antarctic Sectors are shown in Figure 1a. The Antarctic frozen runoff (F_{FR}) used in the CONTROL is approximately equal to the F_{FR} used in the iceberg runs (within 3%), and is shown in Figure 2b. Note that as the calving length decreases to zero, the iceberg meltwater flux, F_{IM}, approaches F_{FR} in all sectors (i.e., the iceberg transport between sectors approaches zero).

3.1. Single *Iceberg Class* (DELTA) Experiments
3.1.1. Iceberg Trajectories and Melt Patterns

The initial size of a calving iceberg strongly affects the lifespan of the iceberg, and the position at which the iceberg meltwater enters the ocean. Large icebergs have a longer lifespan than smaller icebergs, which allows them to travel greater distances from their calving origins, and distribute their meltwater over a wider area of the ocean. For example, in the simulations using a single iceberg calving class, icebergs in the Southern Hemisphere with an initial length $L_0 = 1659$ m (DELTA9) have a median lifespan of 9 years, while the smaller icebergs with $L_0 = 62$ m (DELTA1) have a median lifespan of 1 years. The longer lifespan of larger icebergs means that in these single calving class simulations, the equilibrated mass of icebergs in the Southern Hemisphere increases as the iceberg calving size increases (Figure 2a).

After calving, icebergs drift westward in the Antarctic Counter Current (ACoC), steered by ocean currents and coastal winds. The westward movement of icebergs in the ACoC leads to an iceberg mass redistribution between different sectors of the Antarctic coast (Figure 1a). Larger icebergs spend a longer time in the ACoC than smaller icebergs, which means that the larger iceberg simulations have a greater westward iceberg mass transport around Antarctica. As a result, larger iceberg simulations have a larger fraction of the total iceberg mass being located in the EAS, and a smaller fraction of the total iceberg mass being located in the ABRSS, while the mass fraction in the WSS remains largely unchanged (Figure 2a).

The redistribution of iceberg mass between sectors is accompanied by a corresponding redistribution of iceberg meltwater flux between sectors (Figure 2b). While the total Southern Hemisphere meltwater flux into the ocean is approximately the same for all runs (and is approximately equal to F_{FR}), the increased iceberg mass transport in the larger iceberg simulation results in a decreased freshwater flux into the ABRSS, and an increased freshwater flux in the EAS and WSS. Since the CONTRL simulation has no icebergs and F_{FR} melts instantaneously at the coastline, this means that the CONTROL has a larger integrated freshwater flux in the ABRSS and a smaller integrated freshwater flux into the EAS and WSS than any of the iceberg simulations (Figure 2b).

To further analyze the effect of iceberg calving size, we consider in more detail three simulations using iceberg calving lengths $L_0 = 62$ m, $L_0 = 209$ m, and $L_0 = 1659$ m (shown in the three columns of Figures 3–5). Comparing the trajectories of icebergs in these three simulations (Figures 3a–3c), reveals that typical iceberg drift trajectories vary with iceberg size: smaller icebergs move away from the coast, and spread out uniformly around Antarctica (Figure 3a), while larger icebergs tend to stay closer to the coast, usually crossing the continental shelf margin at fixed locations in the Ross and Weddell Seas, and in the vicinity of the
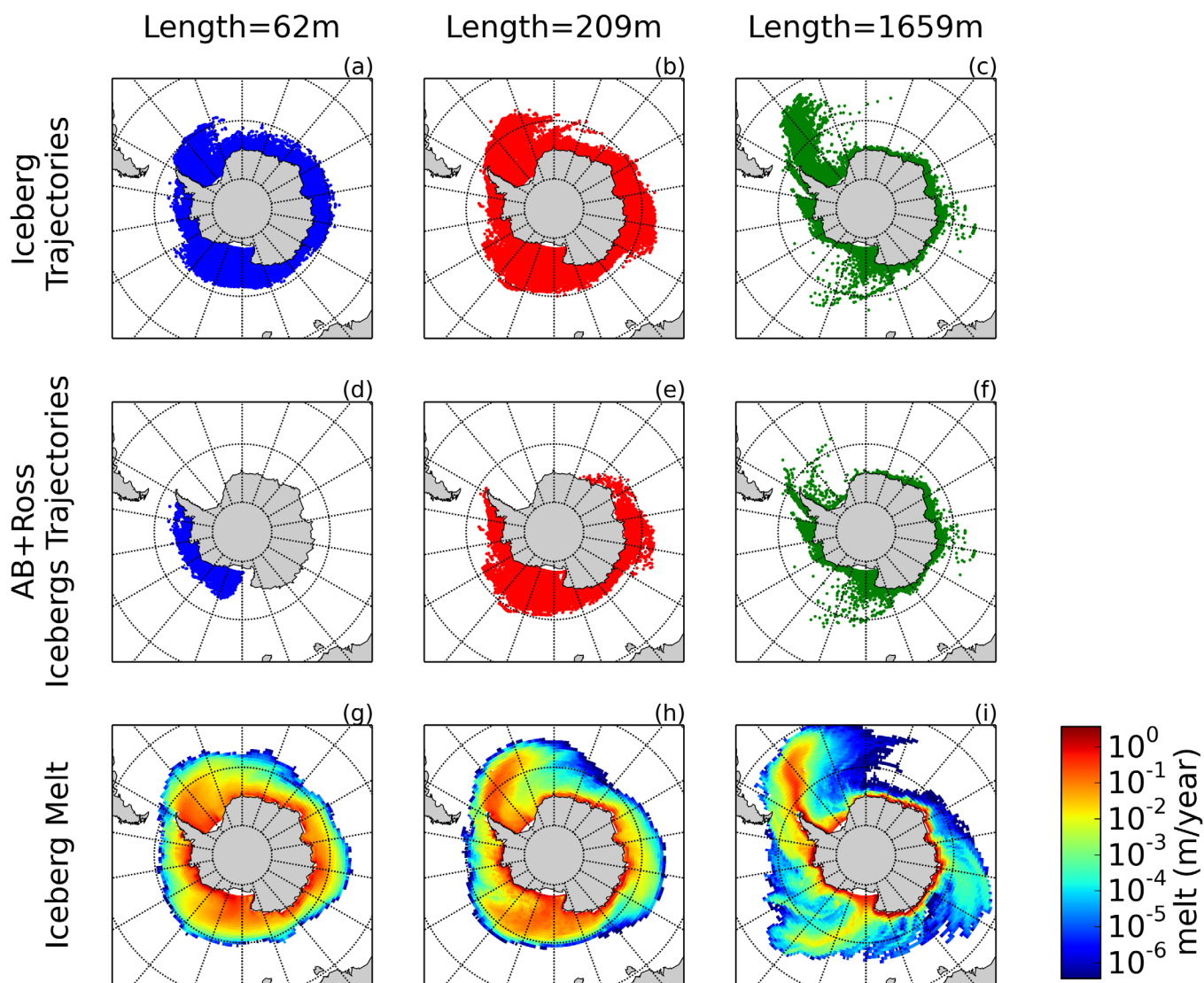
Figure 3. Columns 1, 2, and 3 show iceberg trajectories and melt in experiments with iceberg calving lengths $L_0 = 62$ m, $L_0 = 209$ m, and $L_0 = 1659$ m, respectively. (Row 1) Positions of all Southern Hemisphere icebergs over a 2 year period, sampled monthly. (Row 2) Positions of icebergs calved in the ABRSS over a 2 year period, sampled monthly. (Row 3) Iceberg melt patterns, time-averaged over the final 60 years of the simulation.

Kerguelen Plateau (Figure 3c). These differing trajectories can be understood by considering the magnitudes of the forces acting on the iceberg (equation (2)).

For icebergs moving in the ACoC, the dominant force balance is between (i) the wind drag caused by the westwards wind drifts and northwards Katabatic winds, (ii) the "Coriolis-related force" pushing the iceberg southwards toward the coast, and (iii) the ocean drag force that retards motion [*Gladstone et al.*, 2001]. For smaller icebergs, the wind drag force is larger than the "Coriolis-related force" because the former is proportional to the iceberg surface area, and the latter is proportional to the iceberg mass. For larger icebergs, the "Coriolis-related force" is increasingly dominant. It is thus easier for Katabatic winds to move smaller icebergs northwards out of the ACoC than it is to move larger icebergs. The larger icebergs are mainly driven northwards by current meanders caused by topographic features.

The dependence of westward iceberg transport on calving size is apparent when considering only the icebergs that calve in the ABRSS (shown in Figures 3d–3f). For simulations with larger icebergs, much of the iceberg mass calved in the ABRSS is exported out of the sector before it completely melts (Figure 3f). In contrast, most smaller icebergs melt entirely within the ABRSS (Figure 3d). Remarkably, some large icebergs can
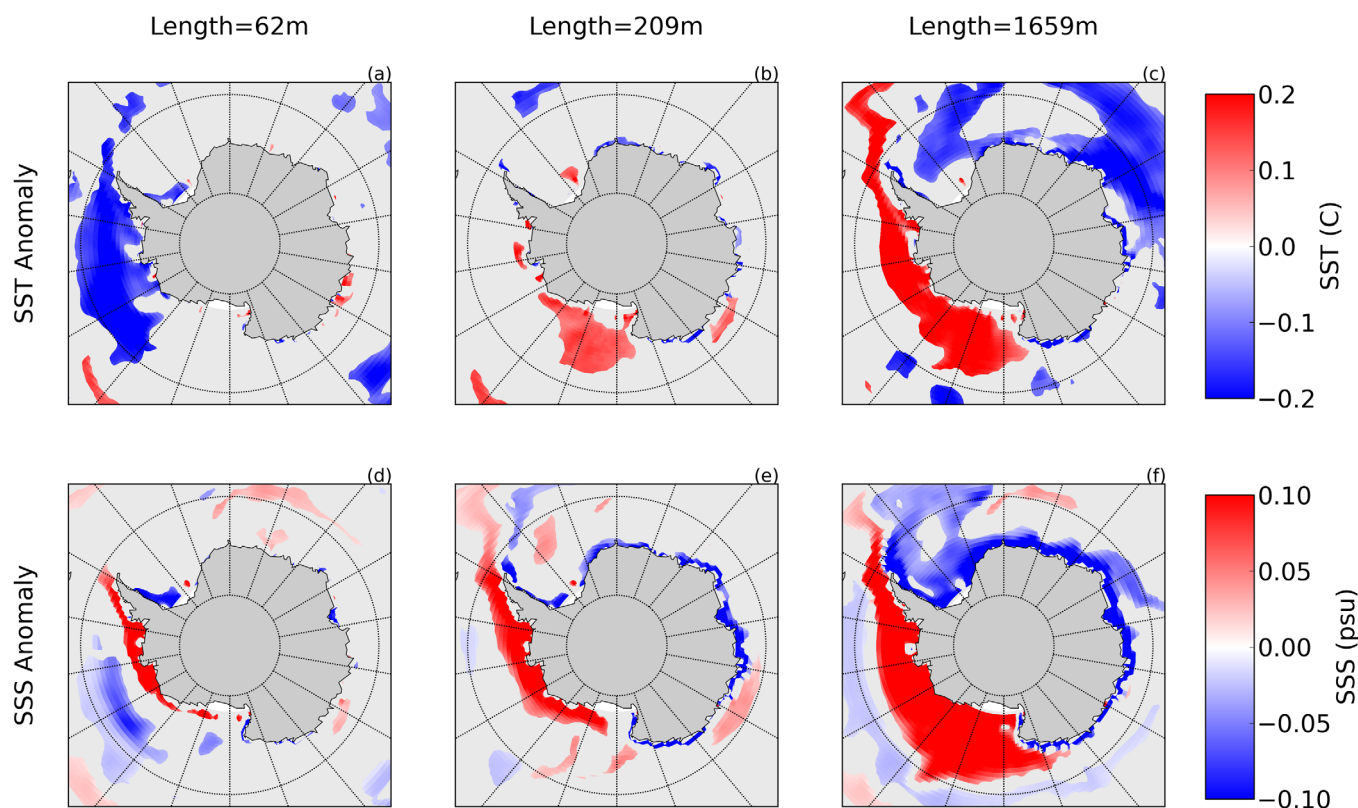
Figure 4. The time-averaged (Row 1) SST and (Row 2) SSS anomalies. Anomalies are relative to the CONTROL simulation (i.e., DELTA—CONTROL). The time averages are taken over the final 60 years of the simulation. Columns 1, 2, and 3 show the results of simulations using calving icebergs with length $L_0 = 62$ m, $L_0 = 209$ m, and $L_0 = 1659$ m, respectively. All colored data are statistically significant at the 95% level, while not statistically significant data are plotted in gray.

drift in the ACoC almost all the way around Antarctica, beginning their journey in ABRSS and eventually reaching the Weddell Sea, where they drift northwards along the east side of the Antarctic peninsula. This feature is also observed in NIC satellite imagery of large ($L \geq 5$ km) Antarctic icebergs [*Stuart and Long*, 2011]. As in the modeling result, large icebergs which calved in the ABRSS sector (plotted in red in Figure 1a) travel long distances in the ACoC, transporting freshwater away from the ABRSS, with some reaching as far as the Weddell Sea.

The differing trajectories of larger and smaller icebergs directly affect the spatial patterns of the iceberg meltwater (Figures 3g–3i). The melt patterns for smaller icebergs are more spatially uniform to the north of the continental shelf than the larger iceberg simulations. Simulations with smaller icebergs have greater meltwater concentrations in much of the region just to the north of the continental shelf margin, but are unable to reach lower latitudes (Figure 3g). In contrast, simulations with larger icebergs produce more melt-water over the continental shelf and at low latitudes (Figure 3i), and also have less meltwater in the ABRSS and more meltwater in the EAS and WSS than simulations with smaller icebergs (Figure 2b).

3.1.2. Ocean and Sea-Ice Impacts

The differing spatial patterns of meltwater flux for simulations with different iceberg calving sizes impacts sea surface temperature (SST) and salinity (SSS) around Antarctica (Figure 4), which, in turn, affects the sea-ice formation (Figure 5). Increased iceberg meltwater flux at the ocean surface causes increased sea-ice growth. This occurs through the following mechanism [*Beckmann and Goosse*, 2003; *Hellmer*, 2004; *Pauling et al.*, 2016]: meltwater at the ocean surface leads to an enhanced stratification in the upper ocean. This increased stratification reduces vertical mixing between the water in the surface mixed layer and the warmer waters below. This reduced supply of heat to the ocean surface promotes sea-ice formation. There are also two additional direct mechanisms linking increased iceberg melt with increased sea-ice formation: (i) the heat required to melt icebergs and the associated cold meltwater cause a cooling of the surface water, which also enhances sea-ice formation, and (ii) the freshwater input from melting icebergs increases
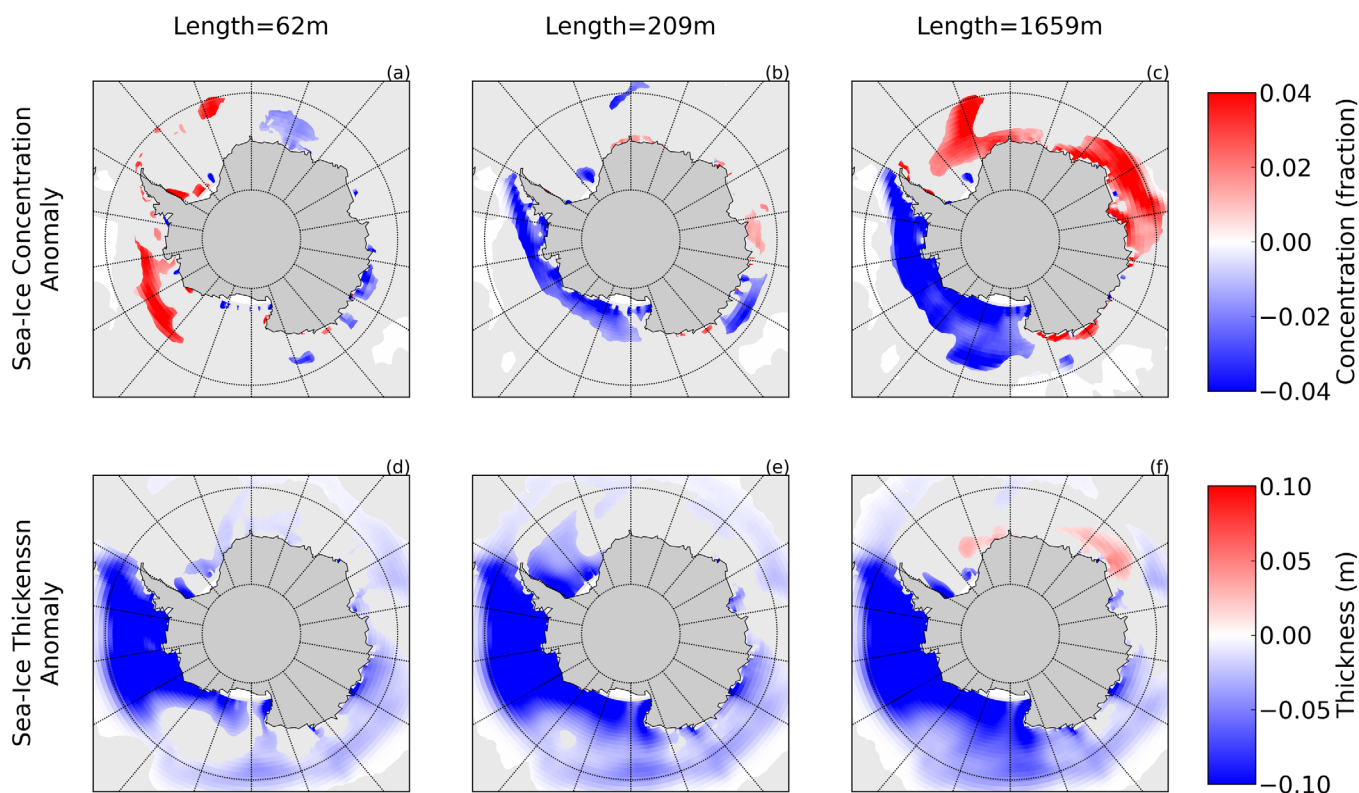
Figure 5. The time-averaged sea-ice (Row 1) concentration and (Row 2) thickness anomalies. Anomalies are relative to the CONTROL simulation (i.e., DELTA—CONTROL). The time averages are taken over the final 60 years of the simulation. Columns 1, 2, and 3 show the results of simulations using calving icebergs with length $L_0 = 62$ m, $L_0 = 209$ m, and $L_0 = 1659$ m, respectively. All colored data are statistically significant at the 95% level, while not statistically significant data are plotted in gray. The sea-ice concentration shows the fraction of a grid cell covered by sea ice.

the (salinity dependent) surface freezing point, which promotes sea ice formation. The changes in sea-ice formation are amplified by a positive feedback between the presence of sea ice and a reduction of the solar insolation, leading to further cooling of the upper ocean, and further sea-ice formation. The converse of these mechanisms also hold: decreased iceberg melt leads to reduced sea-ice formation.

For larger iceberg simulations ($L_0 = 1659$ m), the iceberg freshwater transport out of the ABRSS causes a 33% decrease in the freshwater flux in the ABRSS region relative to the CONTROL simulation (see Figure 2b). This decreased freshwater flux causes positive SST and SSS anomalies (Figures 4c and 4f), and negative sea-ice concentration and thickness anomalies (Figures 5c and 5f) in the ABRSS. A signature of increased subsurface vertical mixing is observed in the ABRSS vertical density transect (Figure 6c), indicated by the dense over fresh anomaly pattern in the upper 1000 m of the ocean. In contrast, for this larger iceberg simulation, the increased meltwater flux in the EAS (41%) and the WSS (57%) relative to the CONTROL simulation cause these sectors to have lower SST's and SSS's (Figures 4c and 4f), less vertical mixing (Figures 6a and 6b), and higher sea-ice concentrations (Figures 5c and 5f). The positive sea-ice anomalies in the EAS and WSS are not as large as the negative anomalies observed in the ABRSS since the increased quantity of meltwater transported into these regions is partially offset by icebergs carrying freshwater away from the coastline, where much of the sea ice is produced.

In experiments with smaller iceberg calving size, the SST and SSS anomalies in the ABRSS sector decrease in magnitude and spatial scale, and for sufficiently small icebergs the sign is reversed (Figures 4a, 4b, and 4d–4e). For the smallest iceberg simulation ($L_0 = 62$ m) the small icebergs effectively move freshwater away from the coast, spreading out uniformly around the continent (Figure 3a). In the ABRSS, this causes a positive salinity anomaly near the coastline, and freshening of the surface water off of the continental shelf (Figure 4d). The increased availability of fresh, cold meltwater offshore leads to increased sea-ice concentrations (Figure 5c), while the increased SSS near the ABRSS coastline causes increased sea-ice production. Since the sea-ice thickness is controlled by the production and export of sea ice near to the coast,
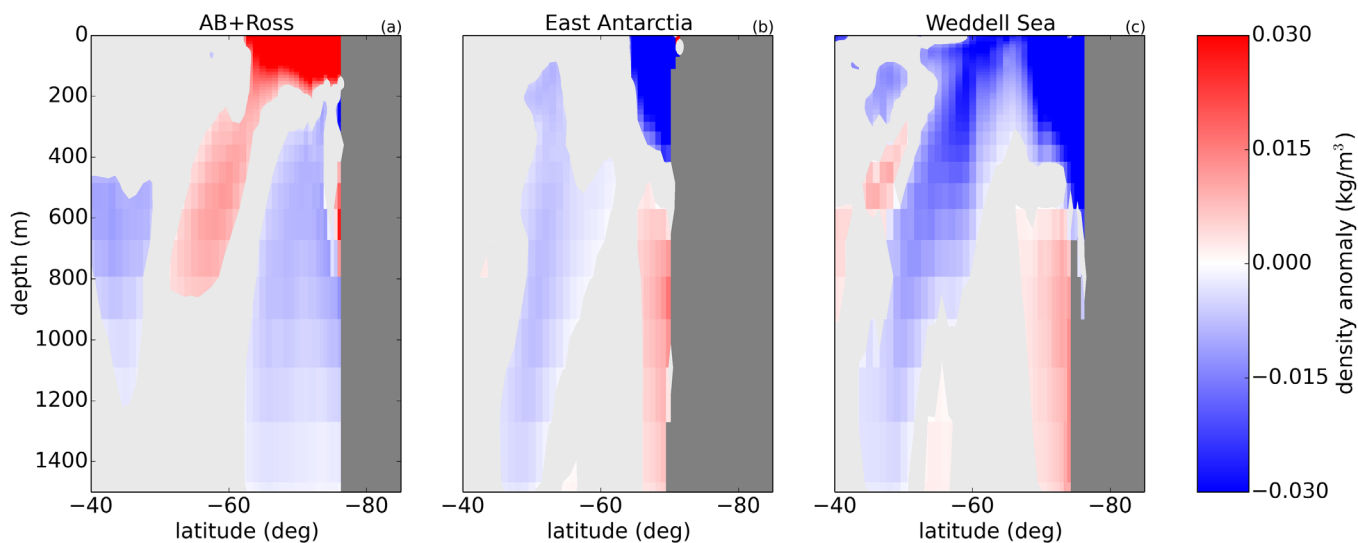
Figure 6. Meridional cross section of the time-averaged density anomalies zonally averaged over the (a) ABRSS, (b) EAS, and (c) WSS regions for the simulations using calving icebergs with length $L_0 = 1659$. Anomalies are taken relative to the CONTROL simulation (i.e., DELTA—CONTROL). The time averages are taken over the final 60 years of the simulation. All colored data are statistically significant at the 95% level, while not statistically significant data are plotted in gray.

we observe decreased sea-ice thickness anomalies in the ABRSS even for the smallest iceberg simulations (Figures 5d–5f). For the smaller icebergs the SSS, SST, and the sea-ice concentration and thickness anomalies in the EAS and WSS are not statistically significant.

We summarize these results by considering the mass of southern hemispheric sea ice in the larger ($L_0 = 1659$ m) and smaller ($L_0 = 62$ m) iceberg simulation relative to the CONTROL simulation. The mass of sea ice in the Southern Hemisphere time-averaged over the final 60 years of the CONTROL simulation is 4.2 $\times 10^{15}$ kg. This amount was reduced for all simulations with icebergs, since icebergs tend to move freshwater away from the continental shelf region where much of the sea ice is formed. For the smaller iceberg simulation, the Southern Hemisphere sea-ice mass was reduced by 6.4%, while the larger iceberg simulation had an 11% reduction. As noted above, the ABRSS sea-ice conditions are most sensitive to iceberg size. In the ABRSS region, the smaller iceberg simulation has a 3.2% decrease in sea-ice mass, while the larger iceberg simulation has an 18% decrease. The sea-ice response in the ABRSS region is largest since the iceberg freshwater transport away from the coast and the iceberg freshwater transport out of the ABRSS (in the ACoC) both lead to a decrease in freshwater over the continental shelf, which is responsible for much of the sea-ice production. In contrast, in the EAS and WSS the smaller iceberg simulation had a 5.5% and 2.1% decrease in sea-ice mass, respectively, while the larger iceberg simulation had a 0.6% increase and 3.8% decrease, respectively. In the large iceberg simulation, in the EAS, the decreases in sea ice associated with introducing icebergs have been entirely offset by the influx of freshwater from the ABRSS to the EAS.

3.2. Composite Experiment

In order to examine the combined effect of icebergs of all sizes, we perform a simulation using a calving-size distribution base on observations of iceberg size frequency. In this COMPOSITE experiment, a calving-size distribution is based on −3/2 power law iceberg-size distributions observed by satellites [*Tournadre et al.*, 2016].

In this experiment, as in previous ones, different trajectories are mapped out by icebergs of different calving size (Figure 7a). Larger icebergs remain close to the coastline, mostly moving northwards when they reach the Weddell Sea, while smaller icebergs cross the shelf break more readily, and are responsible for most of the iceberg melt just offshore of the Antarctic coastline. The melt pattern for the COMPOSITE simulation (Figure 7b) is most similar to the melt pattern from the DELTA9 ($L_0 = 1659$ m) simulation (Figure 3c), which had only the largest icebergs. This is because the −3/2 power law (frequency) spectrum is weighted toward larger icebergs: ∼61% of the iceberg mass is in the largest three iceberg classes, and only ∼6.5% is in the smallest three classes. Similarly, the sea-ice concentration anomalies for the COMPOSITE simulation relative to the CONTROL (Figure 7c), are also similar to those in the larger iceberg simulations (Figure 3i), for the
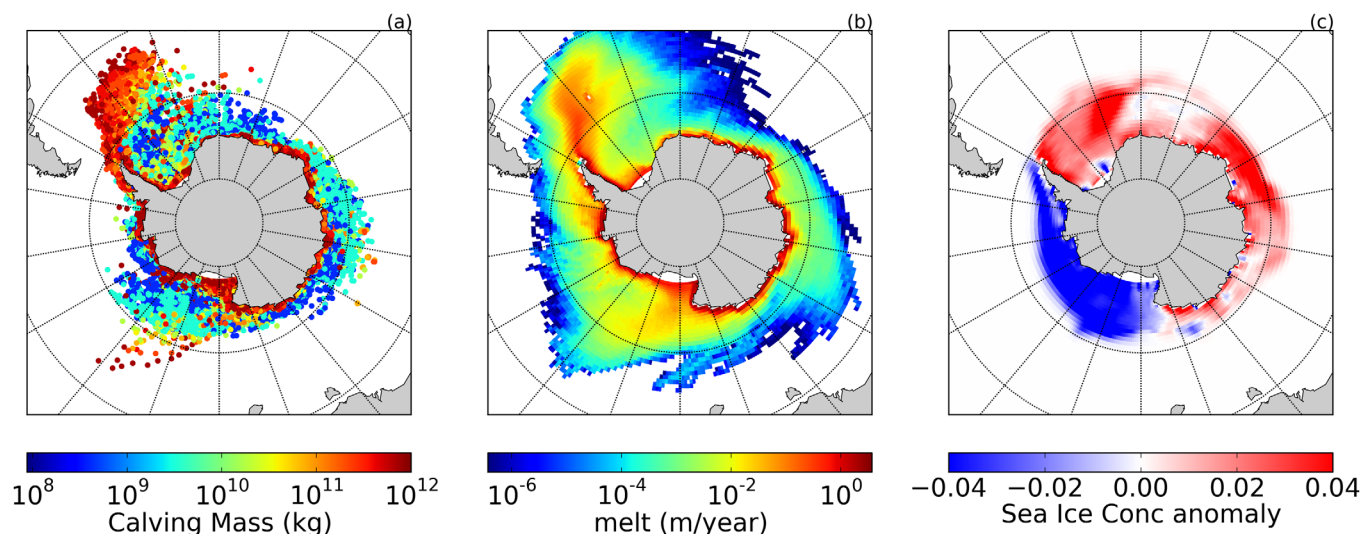
Figure 7. Results for the COMPOSITE simulation. (a) Positions of icebergs over a 2 year period, sampled monthly. The icebergs are colored according to their calving mass. (b) Time-averaged iceberg meltrate. (c) Time-averaged sea-ice concentration anomaly relative to the CONTROL simulation (i.e., COMPOSITE—CONTROL). The time averages are taken over the final 60 years of the simulation.

same reason. The COMPOSITE simulation had an 11% reduction in Southern Hemisphere sea ice relative to the CONTROL simulation. This reduction was dominated by the ABRSS sector which had a 22.3% reduction of sea-ice volume, while the EAS and WSS had a 1.3% increase and 4.9% decrease, respectively, which is again similar to the larger iceberg simulations. The similarity between the COMPOSITE and larger iceberg simulation results suggest that it is more important to focus on modeling larger icebergs since the smaller icebergs account for relatively a small percent of the iceberg mass and ocean/sea-ice response. The differences between the COMPOSITE (iceberg melt only) simulation and the CONTROL (coastal melt only) illustrate the relative role of iceberg melting and coastal melting, and highlight the importance of correctly dividing the Antarctic frozen freshwater flux in climate models into both ice shelf and iceberg melting.

3.3. Comparison to Past Studies

For reference, selected calving-size distributions used in previous studies are shown in Table 2. In the *Martin and Adcroft* [2010] study (and other studies which used the same code), the authors inadvertently interpreted the calving-size distribution G_n [*Gladstone et al.*, 2001], as a mass-weighted distribution, resulting in an effective calving-size distribution, M_n, which is biased toward smaller icebergs (Table 2).

The results in the COMPOSITE simulations agree qualitatively with *Martin and Adcroft* [2010] and *Marsh et al.* [2015] who both reported a decrease in Southern Hemisphere sea-ice volume associated with the presence of icebergs. The spatial pattern of sea-ice anomalies in the COMPOSITE simulation is similar to that of *Martin and Adcroft* [2010], however the fact that the icebergs sizes in that study were heavily weighted to smaller icebergs means that their iceberg simulation is perhaps more readily comparable to the DELTA1 simulation. *Marsh et al.* [2015] reported a 2.9% reduction in Southern Hemisphere sea ice when adding icebergs to their model, which is smaller than the 11% reported here for the COMPOSITE simulation. This large difference is possibly as a result of that study also using an iceberg distribution with too many small icebergs, as in *Martin and Adcroft* [2010]. *Marsh et al.* [2015] also reported increased sea-ice concentrations and thicknesses along the Amundsen and Bellingshausen Seas coastline, which are not observed in this study, and are perhaps due to different model physics.

In addition to the changes in sea-ice concentration and thicknesses, we also observe changes in deep water formation and mixed layer depths associated with introducing icebergs, as reported by *Martin and Adcroft* [2010] and *Marsh et al.* [2015]. These changes in deep water formation are also found to be sensitive to iceberg size, since this controls the freshwater fluxes at the Antarctic coastline. In the COMPOSITE simulation, the changes in mixed layer depth and dense water formation varied regionally, with increased dense water formation and deeper mixed layers in the ABRSS and WSS, and decreased mixed layer depths in the EAS, relative to the CONTROL. Interestingly, the COMPOSITE simulation showed a surface intensified

strengthening of the westward flowing ACoC for the larger iceberg simulations relative to the CONTROL simulation (not shown). In the ABRSS, the ACoC is strengthened at all depths, while in the EAS and WSS the ACoC is strengthened at the surface and reduced at depth. This result disagrees with the result reported in *Marsh et al.* [2015], who observed a strong decrease in the kinetic energy of the ACoC in the East Antarctic region. This suggests that this response is not robust and is model dependent.

3.4. Northern Hemisphere
In the Northern Hemisphere, all the ICEBERG simulations have decreased sea ice thicknesses around Greenland and in Baffin Bay relative to the CONTROL simulation, as was seen in the Southern Hemisphere. Since most icebergs do not enter the Arctic basin, the pack ice in the central Arctic is largely unaffected by adding icebergs to the model. Increasing the size of icebergs leads to an increase in the southward iceberg freshwater flux in Baffin Bay, resulting in decreased SST and SSS along the Eastern Canadian coastline south of Baffin Island. This freshening and cooling of the ocean surface could affect the amount of deep convection, and influence the strength of the Atlantic Meridional Overturning Circulation. Since the region along the Eastern Canadian coastline south of Baffin Island is sea ice free for most of the year, the sea ice conditions in the region are not strongly affected by changing icebergs size (not shown).

4. Iceberg Distributions

The results described above suggest that the calving-size distribution has a significant effect on the model simulations, and omissions of large icebergs introduce biases amplified by feedbacks in the icebergs/sea-ice/ocean interactions discussed above. However, it is still unclear what calving-size distribution should be used for long-term climate simulations. This is a challenging question as the observed iceberg sizes vary over a wide range of scales from tiny bergy bits ($L_0 \leq 10$ m) to giant tabular icebergs ($L_0 \geq 10$ km). The choice of calving-size distribution used in a global climate model should take into account observations, modeled iceberg physics, statistical averages, numerical efficiency, and numerical stability.

4.1. Calving and Open-Ocean Iceberg Distributions
The usual approach in most iceberg modeling studies is to use a calving-size distribution based on the size distribution of icebergs observed in the open ocean [*Gladstone et al.*, 2001; *Martin and Adcroft*, 2010], as was done in the COMPOSITE simulation above. This approach has two advantages: first, satellite observations provide statistics of observed iceberg-size distributions [*Tournadre et al.*, 2016], while there are no direct observations that provide calving-size distributions. Second, since our models do not simulate iceberg breaking, initializing the model with the observed open-ocean size distribution rather than an observed calving-size distribution can be interpreted as a parametrization of the effects of iceberg fracture.

To assess the effect of the prescribed calving-size distribution in the COMPOSITE experiment, we analyze the resultant open-ocean iceberg-size distribution. Figure 8a shows the average iceberg-size distribution for all icebergs in the Southern Hemisphere for the final 60 years of the COMPOSITE simulation. The size distributions for icebergs in each calving-size category are also shown, with the −3/2 line and the prescribed calving-size distribution plotted for reference. Figure 8b shows the same iceberg-size distribution as shown in Figure 8a, but only considering icebergs in the open ocean (in water deeper than 1000 m). The flat distributions observed in both panels for each iceberg class reflect the fact that the model does not contain any iceberg breaking physics. It has been suggested that ice shelf or iceberg breaking (or some other decay process) is needed to achieve the −3/2 power law distribution [*Astrom et al.*, 2006; *Tournadre et al.*, 2016]. However, despite each iceberg class producing a flat iceberg-size distribution, the full iceberg-size distribution (black line) results in a good fit to the −3/2 distribution (dashed line) for areas greater than the area of the smallest iceberg calving class. Hence, prescribing the calving-size distribution using the observed open-ocean distribution is an effective method of achieving the correct open-ocean distribution in the model (within the range of calving sizes used). Note that the agreement between the modeled and observed open-ocean iceberg distribution is not a validation of the iceberg physics, since the open-ocean iceberg distribution is inherited from the calving distribution. However, this result does suggest that the observed −3/2 power law iceberg-size distribution may be due to physics involved in the calving of Antarctic ice shelves, rather than the breaking of icebergs after they have calved. For iceberg areas smaller than the smallest calving size, the full distribution is approximately flat, and does not fit the correct power law
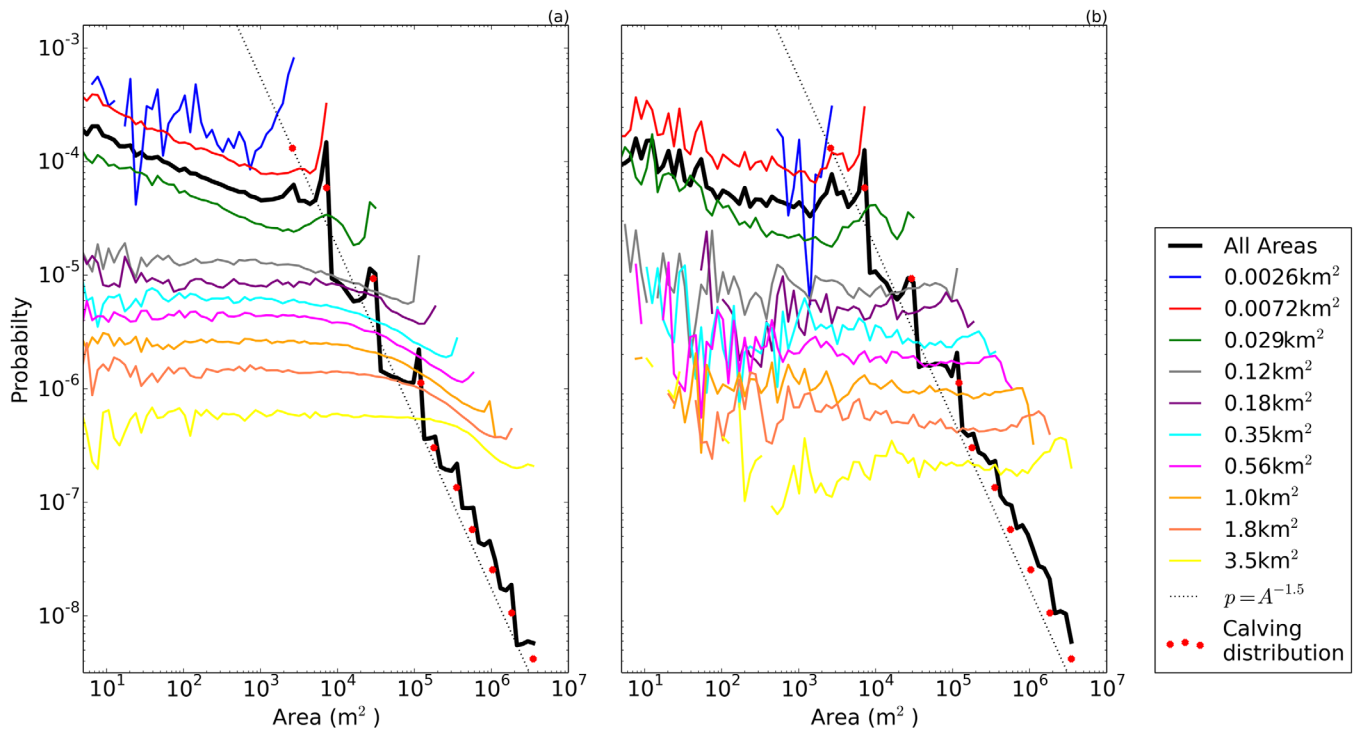
Figure 8. The probability distribution of number of icebergs with a given area found in the COMPOSITE simulation in the Southern Hemisphere over a period of 60 years, sampled monthly. (a) All water depths, (b) water depth greater than 1000 m. The black line shows the distribution of using all icebergs. The colored lines show the same distribution, only considering icebergs in a given calving size class. The red dots show the calving-size distribution used in the COMPOSITE simulation. The dashed line shows the −3/2 power law described in *Tournadre et al.* [2016].

distribution. Since smaller icebergs account for a relatively small percent of the total iceberg mass, having the wrong size distribution for smaller icebergs should not introduce large biases into the model.

4.2. Upper and Lower Bounds for Iceberg-Calving Size

One of the choices made when configuring the iceberg module is the choice of the maximum and minimum iceberg calving-size classes. Choosing a minimum size class that is very small is computationally expensive, since the number of icebergs created and tracked by the model increases as the iceberg size decreases (following the −3/2 power law distribution). This problem has been partially solved by tracking "bundles" of smaller icebergs, where each Lagrangian particle represents a number of icebergs [*Martin and Adcroft*, 2010] (this technique is used in this study with the smallest iceberg size representing 2000 icebergs per particle, see scaling factor in Table 1).

We can estimate the minimum iceberg calving size needed in the model by considering the fraction of the total iceberg mass occupied by icebergs below a given size. If the probability, $p(A)$, of a randomly selected iceberg having an area A, scales like $p(A) \sim A^{-\frac{3}{2}}$, then the corresponding area-weighted distribution, $q(A)$, scales like $q(A) \sim A^{-\frac{1}{2}}$. Including all icebergs with areas, A, less than the maximum area A_{max}, the normalized area-weighted iceberg distribution is given by

$$q(A) = \frac{1}{2} A^{-\frac{1}{2}} A_{max}^{-\frac{1}{2}}. \tag{3}$$

The fraction of the total iceberg surface area accounted for by icebergs with an area $A < A^*$ is

$$\int_0^{A*} q(A) dA = \int_0^{A*} \frac{1}{2} A^{-\frac{1}{2}} A_{max}^{-\frac{1}{2}} dA = \left(\frac{A^*}{A_{max}}\right)^{\frac{1}{2}}. \tag{4}$$

Using the −3/2 power law distribution with a maximum iceberg length of $L_0 = 2285$ m, a fixed iceberg length-to-width ratio of 1.5 and constant iceberg thickness implies that less than 3% of the icebergs mass is contained in icebergs smaller than $L_0 = 62$ m (3% is an over estimate since smaller icebergs tend to be

thinner than larger ones, and allowing for even larger icebergs decreases the importance of the smaller icebergs). Since $L_0 = 62$ m is a computationally feasible lower bound for iceberg size, we conclude that this is a reasonable minimum iceberg size to be used in future climate simulations.

A further question is what is the largest iceberg area that should be used in a climate model? As discussed above, observational evidence suggests that the total iceberg mass is dominated by infrequent large calving events [*Tournadre et al.*, 2016; *Liu et al.*, 2015], which produce giant tabular icebergs much larger than the largest icebergs used in this and other iceberg modeling studies. One extreme example is the giant iceberg with an area of 10,000 km^2 that calved off the Amery Ice Shelf in 1964 [*Fricker et al.*, 2002; *Silva et al.*, 2006]. Using the $-3/2$ iceberg size power law distribution with an upper bound iceberg area of $A_{max} = 10,000$ km^2 would mean that icebergs smaller than $A = 3.5$ km^2 [the largest size iceberg used in this study and many other iceberg studies, *Gladstone et al.*, 2001], would account for less than 2% of the global iceberg mass.

The fact that the iceberg mass flux is dominated by giant icebergs, together with the results from section 3 (showing that iceberg size affects sea-ice and ocean conditions around Antarctica), suggest that it is important that the next generation of iceberg models find a way of including (or parametrizing) the effects of giant icebergs.

4.3. Challenges of Including Giant Icebergs Into Climate Models
There are a number of challenges associated with including giant icebergs into climate models. In this final section, we discuss some strategies for incorporating giant icebergs into climate models, and challenges that need to be overcome. These challenges can be roughly divided into three types: numerical, physical and statistical.

4.3.1. Numerical Issues
Introducing giant icebergs into a climate model leads to a number of numerical complexities, which have to be addressed. First, it is likely that using a Lagrangian point particles is inappropriate to represent giant icebergs (larger than an ocean grid cell), since giant icebergs should be subject to different ocean velocities on different sides of the iceberg. For icebergs larger than the Rossby radius of deformation, the iceberg movement is less sensitive to ocean eddies, so that the icebergs generally follow $^f/_H$ contours [D. MacAyeal, personal communications]. Another difficultly is that the implied volume of a point iceberg can become larger than the volume of an ocean grid column. Since model icebergs should displace the water in a grid cell, using very large icebergs could cause some ocean models to crash (an equivalent problem is found when increasing the ocean model resolution). To address this, icebergs' mass needs to be spread over the appropriate ocean grid points. Allowing the ocean to respond to giant icebergs across multiple grid cells would allow giant icebergs to disrupt flows and change circulations patterns, as is observed in the real-world ocean [*Robinson et al.*, 2010; *Stern et al.*, 2015]. This is especially important in regional models where higher resolution simulations are possible. Finally, since large icebergs are usually thicker, and hence penetrate deeper into the ocean, larger icebergs should be forced by ocean currents integrated over the full iceberg depth, rather than being forced by surface mixed layer currents [*Marsh et al.*, 2015].

4.3.2. Physical Issues
Introducing large icebergs should also be consistent with the model physics. First, giant tabular icebergs are calved only from large Antarctic ice shelves, and cannot be produced by smaller Antarctic ice shelves or in Greenland where the iceberg maximum horizontal dimension is constrained by the width of a fjord (usually ∼5–10 km). Hence, the upper bound for iceberg size needs to be spatially dependent. Second, it is also unclear whether it is physically consistent to represent giant tabular icebergs without including a mechanism for iceberg breakup. For example, a large tabular iceberg that does not break up due to ocean swell, could travel to unrealistically low latitudes. This suggests that parametrization for iceberg breakup need to be introduced at the same time as introducing giant icebergs into the model. Finally, further observations are required to determine whether the $-3/2$ iceberg power law distribution, observed for Southern Hemispheric icebergs [*Tournadre et al.*, 2016], is valid for Northern Hemispheric iceberg distributions.

4.3.3. Statistical Issues
Finally, including giant icebergs into large climate simulations introduces some statistical concerns. The first concern is that the inclusion of the giant icebergs leads to artificial low-frequency variability due to the discretization of the calving-size distribution (i.e., giant iceberg calving at perfectly regular intervals). Second, even neglecting the effects of discretization, the introduction of giant icebergs would make the model

dependent on statistically rare events. In this sense the calving of giant icebergs is somewhat analogous to volcano eruption, which are rare events that have a large effect of the atmosphere. It is still unclear how (or whether) infrequent large iceberg calving events should be incorporated into climate simulations and climate projections.

5. Summary

Simulations of an atmosphere-ocean-land-sea-ice model coupled to a Lagrangian point particle iceberg model are used to assess the effect of iceberg calving size on the sea-ice formation and ocean hydrography around Antarctica. Results show that increasing the size of calving icebergs leads to an increase in the westward iceberg freshwater transport around Antarctica, as large icebergs spend a longer time in the ACoC. This iceberg freshwater transport causes increased SST's and SSS's in the Amundsen, Bellingshausen, and Ross Seas, and a cooling and freshening of the surface ocean around the East Antarctic coastline. The increased salinity of the surface waters in the ABRSS in the large iceberg simulation leads to a decrease in sea-ice formation in this region (by decreasing the ocean stratification, which allows heat to mix up more easily from below). In contrast, the cooling and freshening of the sea surface in the EAS and WSS leads to increased sea-ice formation and decreased subsurface mixing. The ABRSS is the sector most strongly affected by increasing the iceberg calving size since the large icebergs increase the flux of freshwater out of the ABRSS, while there is little or no incoming iceberg freshwater flux (since the iceberg transport through the Drake Passage is relatively small).

These results demonstrate the important role that large Antarctic icebergs play in the climate system by moving freshwater around the Antarctic coast. Furthermore, the results reiterate the importance of using an iceberg model to transport calving meltwater into the global ocean, since discharging all the freshwater at the coastline (as was done in the CONTROL simulation) introduces biases into the model. The results show that the modeled sea ice, SST's and SSS's are sensitive to the calving-size distribution. The anomalies introduced by increasing the size of the icebergs are large scale, regionally coherent and are explained by a simple mechanism (i.e., freshwater moving in the ACoC).

Recent satellite observations show that most of the Southern Ocean iceberg mass is in the form of giant icebergs, larger than the icebergs used in this study [*Tournadre et al.*, 2016]. Since the current generation of iceberg models are only able to include calving iceberg smaller than a few kilometers long, our models likely have a systematic "small-iceberg bias." This fact, together with the results above, suggests that many current ocean models may suffer from biases in sea ice, SST and SSS distributions similar to (or stronger than) the anomalies shown in the COMPOSITE or large iceberg simulation in this study. These results motivate the inclusion of large tabular icebergs in global climate models.

References

Astrom, J. A. (2006), Statistical models of brittle fragmentation, *Adv. Phys.*, *55*(3–4), 247–278.

Beckmann, A., and H. Goosse (2003), A parametrization of ice shelf-ocean interaction for climate models, *Ocean Modell.*, *5*(2), 157–170.

Biddle, L. C., J. Kaiser, K. J. Heywood, A. F. Thompson, and A. Jenkins (2015), Ocean glider observations of iceberg-enhanced biological productivity in the northwestern Weddell Sea, *Geophys. Res. Lett.*, *42*, 459–465, doi:10.1002/2014GL062850.

Bigg, G. R., M. R. Wadley, D. P. Stevens, and J. A. Johnson (1997), Modelling the dynamics and thermodynamics of icebergs, *Cold Reg. Sci. Technol.*, *26*(2), 113–135.

Budd, W. F., T. H. Jacka, and V. I. Morgan (1980), Antarctic iceberg meltrates derived from size distributions and movement rates, *Ann. Glaciol.*, *1*, 103–112.

Delworth, T. L., et al. (2006), GFDL's CM2 global coupled climate models. Part I: Formulation and simulation characteristics, *J. Clim. 19*(5), 643–674.

Depoorter, M. A., J. L. Bamber, J. A. Griggs, J. T. M. Lenaerts, S. R. M. Ligtenberg, M. R. van den Broke, and G. Moholdt (2013), Calving fluxes and basal melt rates of Antarctic ice shelves, *Nature*, *502*(7469), 89–92.

Dieckmann, G., G. Rohardt, H. Hellmer, and J. Kipfstuhl (1986), The occurrence of ice platelets at 250 m depth near the Filchner Ice Shelf and its significance for sea ice biology, *Deep Sea Res., Part A.*, *33*(2), 141–148.

Dinniman, M. S., J. M. Klinck, and W. O. Smith, Jr. (2007), Influence of sea ice cover and icebergs on circulation and water mass formation in a numerical circulation model of the Ross Sea, Antarctica, *J. Geophys. Res.*, *112*, C11013, doi:10.1029/2006JC004036.

Dunne, J. P., et al. (2012), GFDL's ESM2 global coupled climate-carbon Earth System Models. Part I: Physical formulation and baseline simulation characteristics, *J. Clim.*, *25*(19), 6646–6665.

Fricker, H. A., N. W. Young, I. Allison, and R. Coleman (2002), Iceberg calving from the Amery ice shelf, East Antarctica, *Ann. Glaciol.*, *34*(1), 241–246.

Gladstone, R. M., G. R. Bigg, and K. W. Nicholls. (2001), Iceberg trajectory modeling and meltwater injection in the Southern Ocean (19782012), *J. Geophys. Res.*, *106*(C9), 19,903–19,915.

Grosfeld, K., M. Schrder, E. Fahrbach, R. Gerdes, and A. Mackensen (2001), How iceberg calving and grounding change the circulation and hydrography in the Filchner Ice Shelf? Ocean System, *J. Geophys. Res.*, *106*(C5), 9039–9055.

Hellmer, H. H. (2004), Impact of Antarctic ice shelf basal melting on sea ice and deep ocean properties, *Geophys. Res. Lett.*, *31*, L10307, doi: 10.1029/2004GL019506.

Jenkins, A. (1991), A one-dimensional model of ice shelf-ocean interaction, *J. Geophys. Res.*, *96*(C11), 20,671–20,677.

Jongma, J. I., E. Driesschaert, T. Fichefet, H. Goosse, and H. Renssen (2009), The effect of dynamic-thermodynamic icebergs on the Southern Ocean climate in a three-dimensional model, *Ocean Modell.*, *26*, 104–113.

Kusahara, K., H. Hasumi, and G. D. Williams (2011), Impact of the Mertz Glacier Tongue calving on dense water formation and export, *Nat. Commun.*, *2*, 159.

Liu, Y., J. C. Moore, X. Cheng, R. M. Gladstone, J. N. Bassis, H. Liu, J. Wen, and F. Hui (2015), Ocean-driven thinning enhances iceberg calving and retreat of Antarctic ice shelves, *Proc. Natl. Acad. Sci. U. S. A.*, *112*(11), 3263–3268.

MacAyeal, D. R. (1984), Thermohaline circulation below the Ross ice shelf: A consequence of tidally induced vertical mixing and basal melting, *J. Geophys. Res.*, *89*, 597–606.

Marsh, R., et al. (2015), NEMOICB (v1. 0): Interactive icebergs in the NEMO ocean model globally configured at eddy-permitting resolution, *Geosci. Model Dev.*, *8*(5), 1547–1562.

Martin, T., and A. Adcroft (2010), Parameterizing the fresh-water flux from land ice to ocean with interactive icebergs in a coupled climate model, *Ocean Modell.*, *34*(3), 111–124.

Neshyba, S. (1977), Upwelling by icebergs, *Nature*, *267*, 507–508.

Nicholls, K. W., S. Østerhus, and K. Makinson (2009), Ice-Ocean processes over the continental shelf of the southern Weddell Sea, Antarctica: A review, *Rev. Geophys.* *47*, RG3003, doi:10.1029/2007RG000250.

Nøst, O. A., and Østerhus (1998), Impact of grounded icebergs on the hydrographic conditions near the Filchner Ice Shelf, in *Ocean, Ice, and Atmosphere: Interactions at the Antarctic Continental Margin*, edited by S. S. Jacobs and R. F. Weiss, pp. 267–284, AGU, Washington, D. C.

Orheim, O. (1980), Physical characteristics and life expectancy of tabular Antarctic icebergs, *Ann. Glaciol.*, *1*, 11–18.

Pauling, A. G., C. M. Bitz, I. J. Smith, and P. J. Langhorne (2016), The response of the Southern Ocean and Antarctic Sea Ice to fresh water from Ice Shelves in an earth system model, *J. Clim.*, *29*(5), 1655–1672.

Rignot, E., S. Jacobs, J. Mouginot, and B. Scheuchl (2013), Ice-shelf melting around Antarctica, *Science*, *341*(6143), 266–270.

Robinson, N. J., M. J. M. Williams, P. J. Barrett, and A. R. Pyne (2010), Observations of flow and ice-ocean interaction beneath the McMurdo Ice Shelf, Antarctica, *J. Geophys. Res.*, *115*, C03025, doi:10.1029/2008JC005255.

Robinson, N. J., and M. J. M. Williams (2012), Iceberg-induced changes to polynya operation and regional oceanography in the southern Ross Sea, Antarctica, from in situ observations, *Antarct Sci.*, *24*(5), 514–526.

Scambos, T. A., J. A. Bohlander, C. U. Shuman, and P. Skvarca (2004). Glacier acceleration and thinning after ice shelf collapse in the Larsen B embayment, Antarctica, *Geophys. Res. Lett.*, *31*, L18402, doi:10.1029/2004GL020670.

Silva, T. A. M., G. R. Bigg, and K. W. Nicholls (2006), Contribution of giant icebergs to the Southern Ocean freshwater flux, *J. Geophys. Res.*, *111*, C03004, doi:10.1029/2004JC002843.

Smith, K. L., B. H. Robison, J. J. Helly, R. S. Kaufmann, H. A. Ruhl, T. J. Shaw, B. S. Twining, and M. Vernet (2007), Free-drifting icebergs: Hotspots of chemical and biological enrichment in the Weddell Sea, *Science*, *317*, 478–482.

Spahn, F., E. V. Neto, A. H. F. Guimarães, A. N. Gorban, and N. V. Brilliantov (2014), A statistical model of aggregate fragmentation, *New J. Phys.*, *16*(1), 013031.

Stephenson, G. R., Jr., J. Sprintall, S. T. Gille, M. Vernet, J. J. Helly, and R. S. Kaufmann (2011), Subsurface melting of a free-floating Antarctic iceberg, *Deep Sea Res., Part II*, *58*(11–12), 1336–1345.

Stern, A. A., et al. (2015), Wind-driven upwelling around grounded tabular icebergs, *J. Geophys. Res. Oceans*, *120*, 5820–5835, doi:10.1002/2015JC010805.

Stuart, K. M., and D. G. Long (2011), Tracking large tabular icebergs using the SeaWinds Ku-band microwave scatterometer, *Deep Sea Res., Part II*, *58*(11), 1285–1300.

Tournadre, J., K. Whitmer, and F. Girard-Ardhuin (2008), Iceberg detection in open water by altimeter waveform analysis, *J. Geophys. Res.*, *113*, C08040, doi:10.1029/2007JC004587.

Tournadre, J., N. Bouhier, F. Girard-Ardhuin, and F. Rmy (2015), Large icebergs characteristics from altimeter waveforms analysis, *J. Geophys. Res. Oceans*, *120*, 1954–1974, doi:10.1002/2014JC010402.

Tournadre, J., N. Bouhier, F. Girard-Ardhuin, and F. Rmy (2016), Antarctic icebergs distributions 1992–2014, *J. Geophys. Res. Oceans*, *121*, 327–349, doi:10.1002/2015JC011178.

Vernet, M., et al. (2012), Islands of ice: Influence of free-drifting Antarctic icebergs on pelagic marine ecosystems, *Oceanography*, *25*(3), 38–39.

Wadhams, P. (1988), Winter observations of iceberg frequencies and sizes in the South Atlantic Ocean, *J. Geophys. Res.*, *93*(C4), 3583–3590.

Wagner, T. J., P. Wadhams, R. Bates, P. Elosegui, A. Stern, D. Vella, E. P. Abrahamsen, A. Crawford, and K. W. Nicholls (2014), The footloose mechanism: Iceberg decay from hydrostatic stresses, *Geophys. Res. Lett.*, *41*, 5522–5529, doi:10.1002/2014GL060832.